Arabian Journal of Chemistry (2023) **16**, 104539

King Saud University

Arabian Journal of Chemistry

www.ksu.edu.sa
www.sciencedirect.com

ORIGINAL ARTICLE

Aggregation process of fine hematite particles suspension using xanthan gum in the presence of Fe(III)

Zhichao Yang *, Yingqi Han, Qing Teng, Guoyang Zhang, Shengyu Liu

College of Mining Engineering, Taiyuan University of Technology, Taiyuan 030024, China

Received 30 September 2022; accepted 31 December 2022
Available online 5 January 2023

KEYWORDS

Aggregation;
Xanthan gum;
Hematite;
Fe^{3+};
Coordination;
Bridging

Abstract Aggregation is an economical and widely existing method to in hematite mineral processing. In order to achieve the aggregation of hematite particles, high-efficiency agents are required. In this work, the xanthan gum (XG) and Fe^{3+} were used to explore its aggregation effect on the fine hematite particles. The settling and adsorption experiments were conducted on hematite with XG in the absence and presence of Fe^{3+}. The results show that it is difficult to settle hematite with XG alone, and XG exhibits excellent performance with the mass ratio of 2/1 (XG/ $FeCl_3$) at pH 2–10 in the presence of Fe^{3+}. Zeta potential measurements, Fourier transform infrared (FTIR), Microscope and X-ray photoelectron spectroscopy (XPS) analyses were performed to detect the underlying mechanism. The zeta potential, solution chemistry and FTIR analyses results show that the co-adsorption of XG, $Fe(OH)_2^+$, $Fe(OH)^{2+}$ and Fe^{3+} is found on hematite surface through specific and electrostatic adsorption, respectively, and the hematite surface is also covered by $Fe(OH)_{3(s)}$ precipitation turned by Fe^{3+}. XPS spectral investigations and microscope observations provide evidence in support of coordination interaction between ferric ions active sites and XG. In addition, the aggregation model of fine hematite particles suspension using XG in the presence of Fe^{3+} was drawn.

1. Introduction

Aggregation is the most important step in the mineral processing technology, such as flotation, settling and dewatering, to beneficiate the low grade and fine disseminated iron ore (Liang et al., 2015). The conventional reverse flotation technology and high gradient magnetic separators (HGMS) equipment for iron ore separation are the most widely utilized, and it is effective to increase the particle size or volume

* Corresponding author.
E-mail address: yangzhichao@tyut.edu.cn (Z. Yang).
Peer review under responsibility of King Saud University.

Production and hosting by Elsevier

https://doi.org/10.1016/j.arabjc.2022.104539
1878-5352

of the mineral particles in the mineral processing for improving the recovery of fine weakly magnetic iron minerals (Li et al., 2019). Aggregation has been extensively adopted to increase the minerals particle size or volume in the mineral processing. Moreover, flocculation is a kind of aggregation, which is highly attractive for the solid–liquid separation when it is used followed by the other separation processes such as concentration, filtration and sedimentation.

Flocculation, which is related to the surface chemical properties of the materials, is a type of aggregation occurs through hydrophobic interaction or bridging surfactant molecules or long chain polymer molecules to the objective minerals (Sato et al., 2004; Li et al., 2020). Hematite flocculation behaviors have been investigated extensively (Ferretti et al., 2003; Tang et al., 2020; Li et al., 2021). The success of flocculation hematite colloid highly depends on the flocculants that are organic or inorganic polymer. For instance, different types of starch, Carboxymethyl Cellulose (CMC) and Guar gum were used in selective flocculant for the recovery of hematite from iron ore slimes (Moreira et al., 2017; Kumar et al., 2018). Polyacrylamide (PAM) is able to produce large flocs for flotation by bridging adsorption, but a large concentration of PAM could lead to an adverse effect on the following flotation processing and takes a long time to degrade in waste water system (Yue et al., 2018). Though the available literature is rich in the information about the flocculation of hematite using flocculant mentioned above, the high molecular weight polymers are difficult to degrade or need to be solubilized at high temperatures, which is costly. Therefore, it is necessary to find a new and efficient flocculant to accelerate settling the fine hematite during the minerals process.

Flocculation experiments and kinetics using bio-flocculant, such as extracellular bacterial proteins and polysaccharides, have also been reported in the literature (Ferretti et al., 2003; Poorni and Natarajan, 2014). In recent years, xanthan gum (XG), the most important and widely produced microbial polysaccharide extracted from Xanthomonas campestris, has been considered as flocculant for selective flocculation synthetic alumina-silica or iron oxide-silica suspensions have been published (Abu et al., 2019; Loganathan and Sankaran, 2016; Loganathan and Sankaran, 2021). Furthermore, XG is non-toxic, environment friendly, biodegradation, and water-soluble anionic polymer consists of active functional groups which are responsible for XG adsorption onto minerals, it is worthy to investigate the flocculation of fine hematite particles in suspension. According to a significant survey of the literature, there is a lack of enough information about the flocculation hematite using XG as flocculant.

Interactions between XG and dissolved Fe from hematite are of particular interest in aggregation. There is evidence that Fe^{3+} can react with XG forming cross-linked structure due to the presence of polar groups in the XG molecular chains, and decreasing the charge density of the XG molecules (Kang et al., 2019; Yang et al., 2023). In essence, Fe^{3+} compete with active sites on the mineral surface for the binding sites of XG. Tao et al found that Fe^{3+} can collapse the network structure of flocculant, and reduce the adsorption amount of flocculant on hematite (Yue et al., 2018). However, the adsorption of Fe^{3+} and its associated hydrolysis species (e.g., $FeOH^{2+}$, $Fe(OH)_2^+$) onto particles surface due to the electrostatic and van der Waals forces have been viewed as a primary mechanism during coagulation, a type of mineral particles aggregation. In fine hematite particles flocculation system, the benefits of metal ions appear to increase in particles surface potential and associated decrease in electrostatic repulsion and compress double layer (Davis and Edwards, 2017). The possible mechanism is the aggregation of hematite using XG in the presence of Fe^{3+} that the formation of the ternary surface complex between hematite, Fe^{3+} and sorbing ligand.

Therefore, in this work, the aggregation behavior of fine hematite using XG in the presence of Fe^{3+} was investigated, and the aggregation mechanism was also discussed. Such a study would facilitate development of the aggregation process of hematite using bio-flocculant with metal ions.

2. Materials and methods

2.1. Materials

The sample of pure hematite used was obtained from Hebei in China. The mineral sample was dry ground and then sieved through 75 μm standard specification sieve. The characteristic of mineral composition and particle size distribution was measured, as shown in Fig. 1. XRD spectrum (showed in Fig. 1 (a)) confirmed that the hematite was the main iron mineral and little quartz was the gangue, and chemical analysis indicated that the purity of hematite was 95.9 %. The XRD and chemical analyses confirm that the purity of hematite sample meets the experimental requirements. The particle size distribution of the hematite sample for the settling experiments measured by Malvern Mastersizer 2000 was shown in Fig. 1(b). It can be seen that the mean diameter of the distribution is 14 μm, and with 50 % of the particles in the slurry having a diameter of less than 10.0 μm and 80 % having a diameter of less than 38 μm. Deionized water, chemically pure $FeCl_3 \dot{s} 6H_2O$ and analytically pure reagents hydrochloric acid (HCl) and sodium hydroxide (NaOH), used as pH regulators, were used in all experiments. XG derived from starch involving a fermentation process by the *Xanthomonas* bacterium was supplied by Shandong Usolf Chemical Technology Co., ltd, China.

2.2. Settling experiments

All experiments were performed in 250 mL graduated cylinder by mixing 10 mg/L of XG and 60 mg/L of $FeCl_3 \dot{s} 6H_2O$ solutions. The 1.0 g of hematite was added into 200 mL deionized water and shaken at a speed of 800 rpm for 2 mins at 25 °C in each experiment. The desired value of pH was achieved by addition of HCl or NaOH. After adding the XG and Fe^{3+} the mixture was stirred at 600 rpm for 4 min and then transferred to a 250 mL graduated cylinder. It should be noted that Fe^{3+} was added into the pulp following with XG. After settling for 1 min, the supernatant at the half-height was withdrawn for weighting separately following filtration and drying, and the settling rate was calculated based on the weight of the products. The settling rate (γ) was defined and calculated by the following formula:

$$\gamma = \frac{m_0 - m_t}{m_0} \times 100\% \quad (1)$$

where m_0 and m_t (g) are the hematite weights at an initial time and sample supernatant, respectively.

2.3. Adsorption tests

All experiments were performed in 250 mL glass flask by mixing XG, 1.0 g of hematite sample and 60 mg/L of the $FeCl_3 \dot{s} 6H_2O$ solutions at nature pH. After adding the XG and $FeCl_3 \dot{s} 6H_2O$, the suspension was then shaken at a speed of 600 rpm for 4 mins using a vortex shaker. Next, the XG concentrations in the supernatant liquor were determined using the phenol sulfuric acid method (Zhang et al., 2020). The adsorption amount of XG ($mg \dot{s} g^{-1}$) was computed as follow.

$$q_t = \frac{C_0 - C_t}{m} V \quad (2)$$

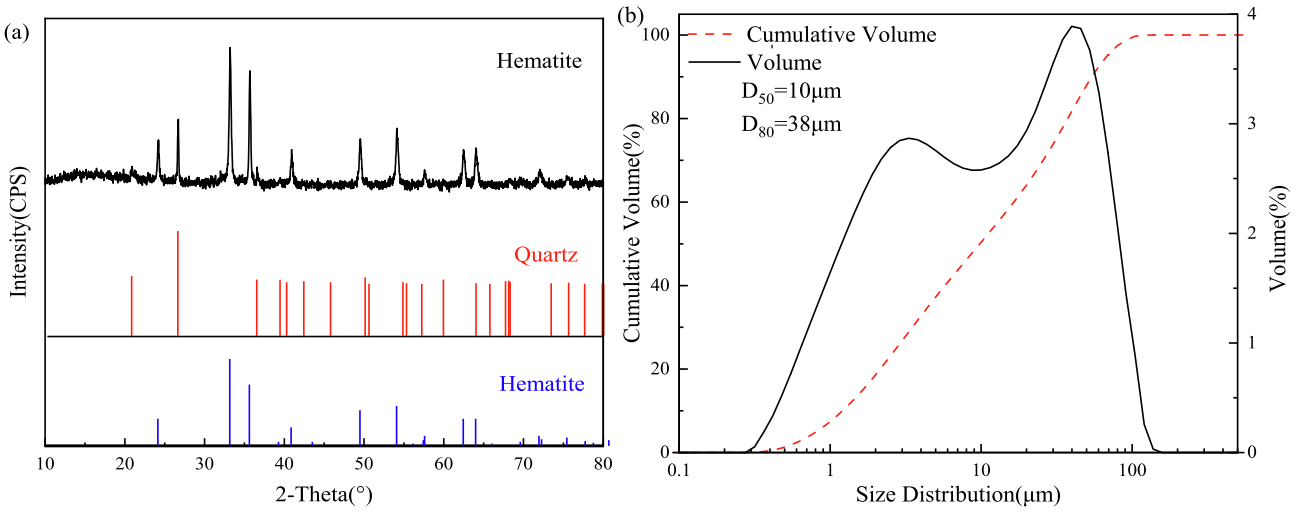

Fig. 1 X-ray diffraction pattern (a) and particle size distribution (b) of the hematite sample.

where C_0 and C_t (mg·L^{-1}) are the XG concentrations at an initial time and equilibrium condition respectively, V (L) is the volume of XG and adsorbent solution and m (g) is the hematite mass.

2.4. Microscope analysis

The aggregation morphology of samples of hematite and adsorption XG on hematite in the absence and presence of Fe^{3+} at pH 6.4 were confirmed using Microscope. The samples from settling experiments were sucked onto a glass slide with a glue tip dropper, and the aggregation morphology was observed under a microscope at different times and the pictures were taken.

2.5. Zeta potential

The zeta potentials of hematite surface were measured using an electrophoresis instrument. The pure hematite sample was ground to −5 μm in an agate mortar. Then the samples were mixed with 10 mg/L of XG solutions in the absence and presence of 60 mg/L $FeCl_3·6H_2O$. After stirring for 5 min, the pH of the suspension was adjusted to the desired value using NaOH or HCl. The suspension was further conditioned and allowed to stand for 5 min until the pH stabilized. Then, the zeta potential was measured and the average of five separate readings and its standard deviation were reported.

2.6. Surface chemical analysis

The aggregation mechanism of XG and Fe^{3+} on hematite was analyzed by Fourier transform infrared spectroscopy (FTIR) and X-ray photoelectron spectroscopy (XPS). The samples preparation process was as same as section 2.4, and the samples were filtered and washed 3 times with deionized water. Finally, the samples were vacuum dried at 50 °C and used for testing. The FTIR spectra were surveyed with an ALPHA-T FTIR spectrometer (Bruker, Germany). The transmission spectroscopy with a wavenumber measurement range of 500–4000 cm^{-1} was applied for the analysis. XPS analysis was characterized by an X-ray photoelectron spectrometer (Thermo Scientific K-Alpha). The peak fitting and data analysis were carried out with XPS software CasaXPS Version 2.3, and all the spectra were charge corrected using the high-resolution C 1 s main component at 284.80 eV.

3. Results and discussion

3.1. Settling studies

The settling rate of hematite suspension as a function of XG dosage, pH, the mass ratio of XG: $FeCl_3·6H_2O$ and adding order of $FeCl_3·6H_2O$ and XG are illustrated in Fig. 2. As seen in Fig. 2(a), the settling rate of hematite increased with the addition of XG concentration from 6 to 10 mg/L, above which the settling rate decreased. Similar results were received by other research; i.e., excessive dosage of bio-flocculant caused re-stabilization of the colloids in the kaolin suspension or coal waste slurry (Bratskaya et al., 2005; Yang et al., 2017). Loganathan and Sankaran have explained the mechanism of flocculation of iron oxide with XG, "bridging flocculation" is responsible for the aggregation of iron oxide (Loganathan and Sankaran, 2021). According to the previous reports, about 50 % coverage of the particle surface by polymer agrees with the optimum concentration of flocculant for the highest settling rate (Yang et al., 2017). When the adsorption of polymer onto solid surface beyond an optimum concentration of flocculant in solution or covered completely with the polymer, steric repulsion would lead to stable suspension. Similarly, Weissenborn has found the optimum concentration of starch flocculant (range of 25 to 50 mg/L) to attain a maximum flocculation hematite and a significant decrease in the flocculation was evidenced beyond 100 mg/L, which was attributed to the steric stabilization (Weissenborn, 1996).

Fig. 2(b) shows the effect of the pH on the settling capabilities of XG to hematite. The settling rates of hematite decreased as the pH increased especially in the pH range from 4.0 to 8.0 when only XG was added to the hematite suspension. A maximum settling rate of 90.4 % was observed at pH 2.0, the highest aggregation of hematite particles due to

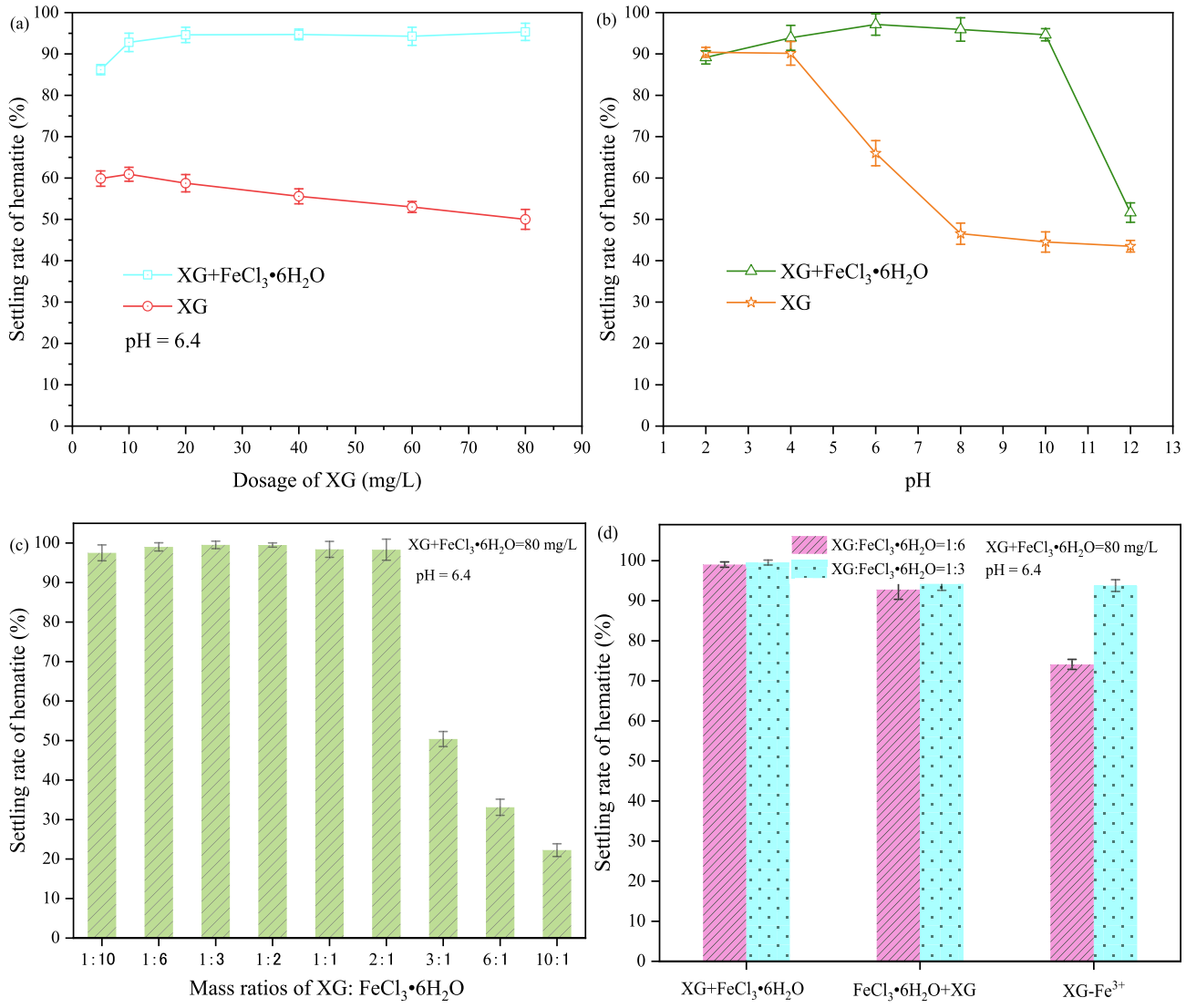

Fig. 2 Settling rates of hematite as a function of XG dosage (a), pH(b), mass ratio of XG:Fe^{3+} (c) and (d) adding order of Fe^{3+} and XG.

electrostatic adsorption between hematite and XG. Hematite particles surface has a positive charge when the value of pH is lower than the isoelectric point (IEP) value of hematite (4.5). The positive charged hematite adsorbs the negative charge of XG which is an anionic polysaccharide through electrostatic interaction (Mittal et al., 2021). The high negative charge of hematite particles in the pH region of 5–12 results in the higher electrostatic repulsion between hematite surface and XG. According to the research of Loganathan and Sankaran and report of Kang et al., XG adsorbs to hematite through chemical complexation between XG and Fe^{3+} on hematite surface (Loganathan and Sankaran, 2021; Kang et al., 2019). Although chemical complexation plays the predominant role in the adsorption of XG onto hematite, the long-range electrostatic interaction may have a temporary adverse impact on short range chemical interaction. In addition, XG suffered competitive adsorption with hydroxyl on the surface of hematite. Consequently, a lower settling rate is observed in these pH ranges.

The addition of XG and $FeCl_3$ś$6H_2O$ on hematite suspension increases the maximum settling rate from 66.0 % to 97.1 % at pH 6.0 and the pH window of high settling has also increased from the pH region of 2–4 to 2–10, as shown in Fig. 2 (a) and (b). These suggested that Fe^{3+} could produce a positive effect on hematite particles aggregation, but the pulp pH has a significant influence. Fe^{3+} and related hydroxyl complex ions $Fe(OH)^{2+}$ and $Fe(OH)_2^+$ species could obviously be decreased or neutralized the negative charge of hematite, this is beneficial to the adsorption of XG onto hematite. Unfortunately, the concentration of Fe^{3+}, $Fe(OH)^{2+}$ and $Fe(OH)_2^+$ species decreased with the increase of pulp pH, while $Fe(OH)_{3(s)}$, $Fe(OH)_{3(aq)}$ and $Fe(OH)_4^-$ species might predominate in alkaline environments, resulting in a decreasing settling rate of hematite (Wang et al., 2021). Furthermore, the high concentration of Fe^{3+} produced a positive effect on hematite particles aggregation, as shown in Fig. 2(c). It can be seen that the settling rate of hematite is only 50.4 % with a mass ratio of 3/1 (XG/ $FeCl_3$ś$6H_2O$) while that is about 98.3 % with a mass

ratio of 2/1(XG/ $FeCl_3$ś$6H_2O$). The results shown in Fig. 2(d) indicate that the addition order of XG and Fe^{3+} has no obvious influence on the hematite particles aggregation. However, the settling rate of the third condition that was mixed with XG and $FeCl_3$ś$6H_2O$ together and then added into the pulp was lower than that of two models of XG following with $FeCl_3$-ś$6H_2O$ and $FeCl_3$ś$6H_2O$ following with XG. The addition of Fe^{3+} could affect XG's fate in the aquatic environment and the form of complex Fe-XG occurs by complexation when $FeCl_3$ś$6H_2O$ and XG were mixed (Kang et al., 2019). It suggests that adding the order of XG and $FeCl_3$ś$6H_2O$ was critical to achieving the hematite particles aggregation effectively.

3.2. Comparison with literatures results

Table 1 lists the flocculation capacities of combination of XG and Fe^{3+} and the other similar materials reported in literatures. By comparing with other flocculants, it can be seen that the XG exhibits strong flocculation capacity. That means XG consists of active functional groups which are easier to interaction with minerals then other flocculant. However, a higher flocculation rate (98 %) was obtained in literature (Loganathan and Sankaran, 2021), and the result is not consistent with the results in Fig. 2. Because the study was conducted using chemically synthetic iron oxides, and it is clear that there must be large differences in surface properties between these chemical compositions and minerals. Furthermore, the combination of XG and Fe^{3+} exhibits higher aggregation capacity for the hematite suspension settling than single XG.

3.3. Adsorption studies

To verify the enhancement of XG adsorption on hematite in the presence of Fe^{3+}, the actual adsorption capacity of XG on hematite was measured at nature pH 6.4 and the results are shown in Fig. 3. Considering the effect of pH and the mass ratio of Fe^{3+} to XG, nature pH and 60 mg/L of $FeCl_3$ś$6H_2O$ were employed to carry out the adsorption investigation. It can be seen that Fe^{3+} exhibits a good enhancement for the adsorption capacity of XG on hematite. The addition of 60 mg/L of $FeCl_3$ś$6H_2O$ increased XG adsorption on hematite so that the adsorption capacity was increased from 5.4 to 20.9 mg/g when the concentration of XG was 80 mgśL^{-1}. These results are in agreement with the settling results shown in Fig. 2(a) and (b). This was likely caused by the co-adsorption of XG and Fe^{3+} on the hematite surface. Fe^{3+} can adsorbs on the hematite surface through electrostatic adsorption, and XG

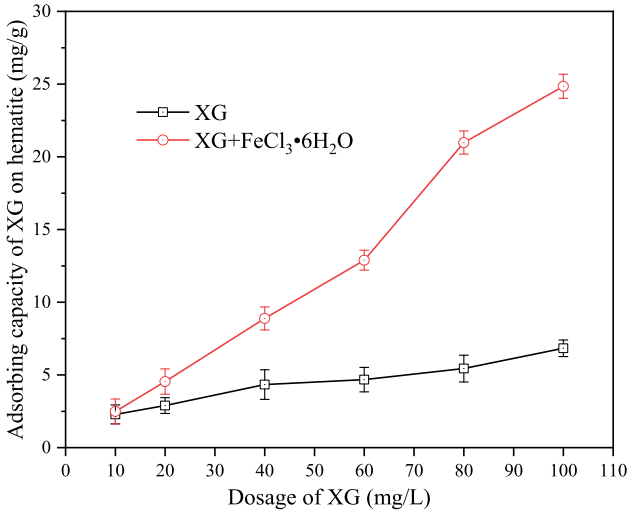

Fig. 3 Adsorption capacity of XG on hematite as a function of XG dosage in the absence and presence of 60 mg/L $FeCl_3$ś$6H_2O$ at pH 6.4.

molecules are adsorbed on the hematite surface through electrostatic adsorption and complexation happened between active species of XG with Fe^{3+}. The positive charged Fe^{3+} is bound to the negative position on hematite, which increases the active Fe sites on hematite surface and reduces the electrostatic repulsions between XG and hematite.

3.4. Zeta potential and solution chemistry studies

The surface charge is widely used to characterize the interaction between minerals and reagents. Therefore, the zeta potential values of hematite as a function of pH in the absence and presence of XG and Fe^{3+} were measured, as shown in Fig. 4. As can be seen, the IEP of hematite occurred at about pH 4.5, consistent with previous reports (Wang et al., 2021; Zhang et al., 2017). With either XG or $FeCl_3$ś$6H_2O$ added, the IEP of hematite shifted to lower or higher pH values, suggesting that both XG and Fe^{3+} could adsorb onto the hematite surface. Similar phenomena have been reported in iron oxide-XG and hematite-Fe^{3+} systems (Yue et al., 2018; Loganathan and Sankaran, 2021). This behavior may be attributed to the negative charge of XG adsorption onto the hematite through chemical complexation, and charge neutralization is the main mechanism for Fe^{3+} adsorption onto

Table 1 Comparison of aggregation capacities between XG and literatures.

Flocculant	Flocculation rates /%	Reference
PAM + KNO_3	55	(McGuire et al., 2006)
Dextrin	75	(Li et al., 2021)
Polyethylene oxide (PEO)	95	(Li et al., 2021)
Guar gum	60	(Jain et al., 2017)
Degraded wheat starch	90	(Panda and PradipK. Banerjee, Surendra Kumar Biswal, R. Venugopal, N.R. Mandre. , 2013)
XG	98	(Loganathan and Sankaran, 2021)
XG - Fe(III)	99	This study

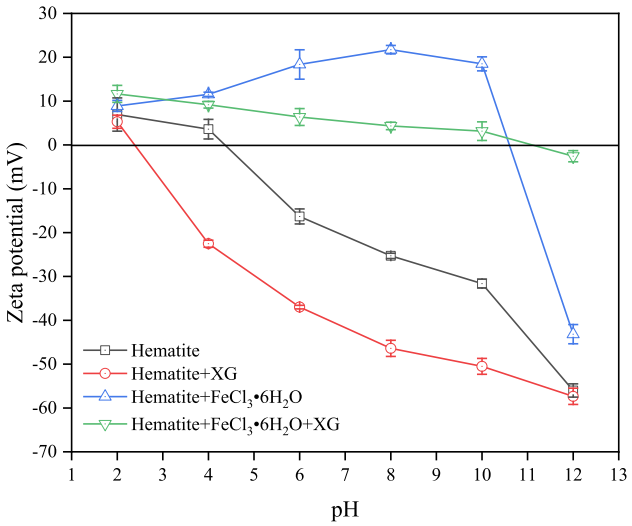

Fig. 4 Zeta potential of hematite as a function of pH in the absence and presence of XG and $FeCl_3 \dot{s} 6H_2O$.

hematite surface. Moreover, when $FeCl_3 \dot{s} 6H_2O$ was added into the pulp following with XG, the zeta potential of hematite was not as positive as that hematite interacted with Fe^{3+} in the pH range from 4 to 10, indicating that the co-adsorption of XG and Fe^{3+} on hematite surface occurred. According to the previous reports, XG contains a large number of polar groups, such as hydroxy and carboxyl groups, which could coordinate with Fe^{3+} to form coordination complexes (Loganathan and Sankaran, 2016; Kang et al., 2019). However, the zeta potential of hematite with XG or $FeCl_3 \dot{s} 6H_2O$ added changed little at pH 12, indicating that adsorption XG and Fe^{3+} on hematite was different. This is in agreement with the settling results shown in Fig. 2(b).

In the solution with different pH values, the species and the content of the species in the presence of 0.5×10^{-3}mol/L Fe^{3+} ions were calculated using the stability constants for hydroxide formation, and the results are shown in Fig. 5. Although the species of Fe^{3+}, $Fe(OH)^{2+}$ and $Fe(OH)_2^+$ are widely distributed at pH 0–8, the species of $Fe(OH)_{3(s)}$ is the main species when pH value exceed 2.17. The concentration of Fe^{3+}, $Fe(OH)^{2+}$ and $Fe(OH)_2^+$ are 1.0×10^{-15} mol/L, 1.0×10^{-11} mol/L and 1.0×10^{-8} mol/L, respectively at pH 6.4, and the distribution concentration of them are lower than that of $Fe(OH)_{3(s)}$ and $Fe(OH)_{3(ag)}$. Therefore, zeta potential of hematite with adding $FeCl_3 \dot{s} 6H_2O$ at a pH range from 2 to 8 increasing is mainly attributed to $Fe(OH)_{3(s)}$ covering and the adsorption of $Fe(OH)_2^+$, $Fe(OH)^{2+}$ and Fe^{3+}. Studies reported that the interaction between XG and Fe^{3+} could cause expansions of the XG molecule chains at a pH range from 3 to 10, resulting in swelling of XG-Fe(III) hydrogels (Liu et al., 2017; Rahbari et al., 2017). So, the XG molecules could coordinate with Fe^{3+} in the solution with different pH values even when Fe^{3+} turned to $Fe(OH)_{3(s)}$ and $Fe(OH)_{3(ag)}$ at alkali pH. The enhancement of adsorption XG onto hematite surface by Fe^{3+} at pH 6.4 in Fig. 3 is attributed to XG coordination with precipitation of colloidal $Fe(OH)_3$ which could adsorb on the surface of hematite particles. Also, $Fe(OH)_4^-$ seems can't form complexes with the anionic polysaccharide XG, and this phenomenon agrees with the results of settling rate of hematite decreasing at a pH range from 10 to 12 in Fig. 2(b).

3.5. FTIR analysis

The FTIR spectra of XG, hematite and adsorption XG on hematite in the absence and presence of Fe^{3+} are shown in Fig. 6. In the case of XG powder, XG spectra with a broad absorption peak at 3435 cm^{-1} related to the stretching vibration of the –OH group, as extensively reported in the literature (Kang et al., 2019). The peak at 2920 cm^{-1} corresponds to the strongly hydrogen bonded–OH groups (Loganathan and Sankaran, 2021). The two small bands at 1732 cm^{-1} and 1626 cm^{-1} are related in several studies to the stretching of carbonyl (C═O) of the acetyl groups and asymmetrical stretching

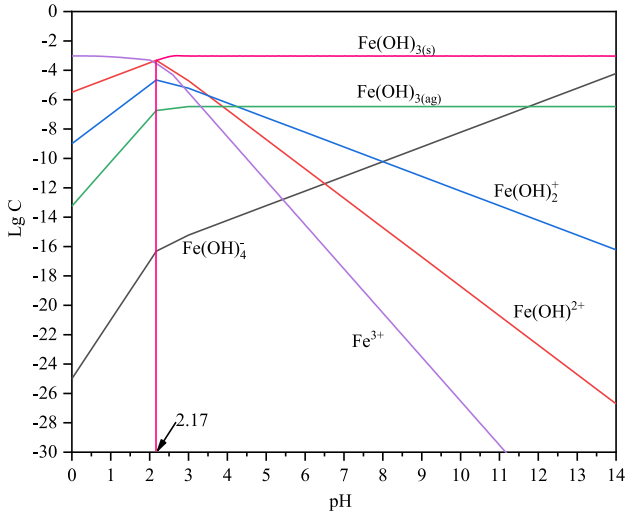

Fig. 5 Species distribution diagrams of ferric ions as a function of pH (C_T: 0.5×10^{-3} mol/L).

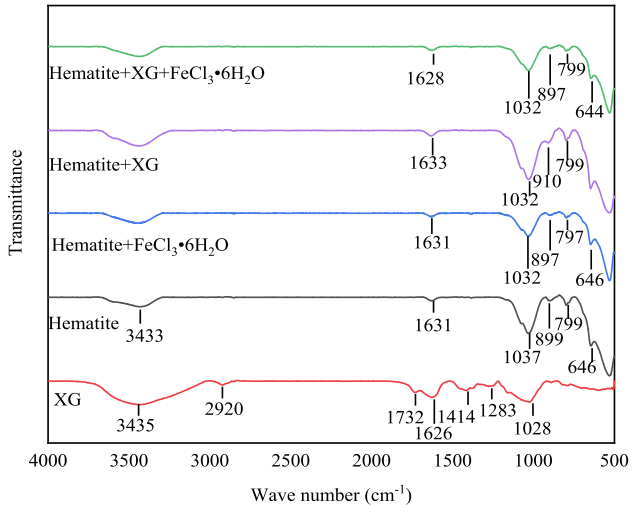

Fig. 6 FTIR spectrum of XG, hematite and adsorption XG on hematite in the absence and presence of $FeCl_3 \dot{s} 6H_2O$ at pH 6.4.

of the C═O group of pyruvate groups, respectively (Mittal et al., 2021; Duczmal et al., 2005). The bands that appear at 1414 cm^{-1} and 1028 cm^{-1} are assignable to the symmetrical stretching of the $–COO^-$ group of glucuronic acid and -C-OH deformation vibrations, respectively. The FTIR spectrum of hematite is also portrayed in Fig. 6. The intense band at 1037 cm^{-1}, 899 cm^{-1} and 580 cm^{-1} are attributable to Fe-O stretching vibrations. The small band that appears at 1631 cm^{-1} is due to the –OH scissoring vibrations from the moisture. Similarly, the broad absorption peak that appears at 3433 cm^{-1} corresponds to the –OH stretching vibrations. The assignments of the functional groups made for hematite samples are in reasonable agreement with those reported in the literature (Moreira et al., 2017; Loganathan and Sankaran, 2021; Salam et al., 2015).

In the case of hematite interacting with XG, the band at 899 cm^{-1} assigned to the Fe-O stretching vibrations of hematite is shifted to 910 cm^{-1} after interaction with XG, which can be attributed to the chemical interaction between hematite and XG. This agrees with the results of Zeta potential analysis that indicate the negative charge of XG adsorption onto the hematite through chemical complexation. The peak at 1028 cm^{-1} assigned to -C-OH deformation vibrations of XG coupled to Fe-O stretching vibrations of hematite observed at 1037 cm^{-1} appears at 1032 cm^{-1} in case of hematite interacted with XG, suggesting the hydrogen bonding between hematite and XG. Therefore, the most pronounced changes in XG adsorbed on hematite are linked to Fe-O and -C-OH stretching vibrations modes, suggesting that XG adsorption onto hematite surface may occur through these functional groups. The peak at 799 cm^{-1} assigned to Fe—O—H vibration of hematite has shifted faintly and appears at 797 cm^{-1} after interaction with Fe^{3+}. Similarly, the peak at 1037 cm^{-1} to assigned to Fe-O stretching vibrations shifted to 1032 cm^{-1} in case of hematite interacted with Fe^{3+}. These changes suggest the formation of a goethite-like surface since the Fe—O—H and Fe-O bending vibration are related to the goethite phase (Moreira et al., 2017). According to the results of solution chemistry calculating, the species of $Fe(OH)_{3(s)}$ and $Fe(OH)_{3(ag)}$ are the main species at pH 6.4. This means that the hematite surface is covered by $Fe(OH)_{3(s)}$ precipitation and/or adsorbs $Fe(OH)_{3(ag)}$, $Fe(OH)_2^+$, $Fe(OH)^{2+}$ and Fe^{3+} when $FeCl_3 \dot{s} 6H_2O$ is added into the hematite pulp at pH 6.4. In the case of hematite interacting with XG and $FeCl_3 \dot{s} 6H_2O$, the adsorption of XG onto hematite occurred through chemical and hydrogen bonding since the two bands at 1037 cm^{-1} and 899 cm^{-1} have shifted. But it is not confirmed that a goethite-like surface forms because the peak at 799 cm^{-1} assigned to Fe—O—H vibration of hematite has not shifted. This may be attributed to the result of the complexation between XG and Fe^{3+}. The FTIR results were in line with the data shown in the zeta potential tests.

3.6. Microscope analysis

Microscope was utilized to observe the aggregation morphology of hematite and adsorption XG on hematite in the absence

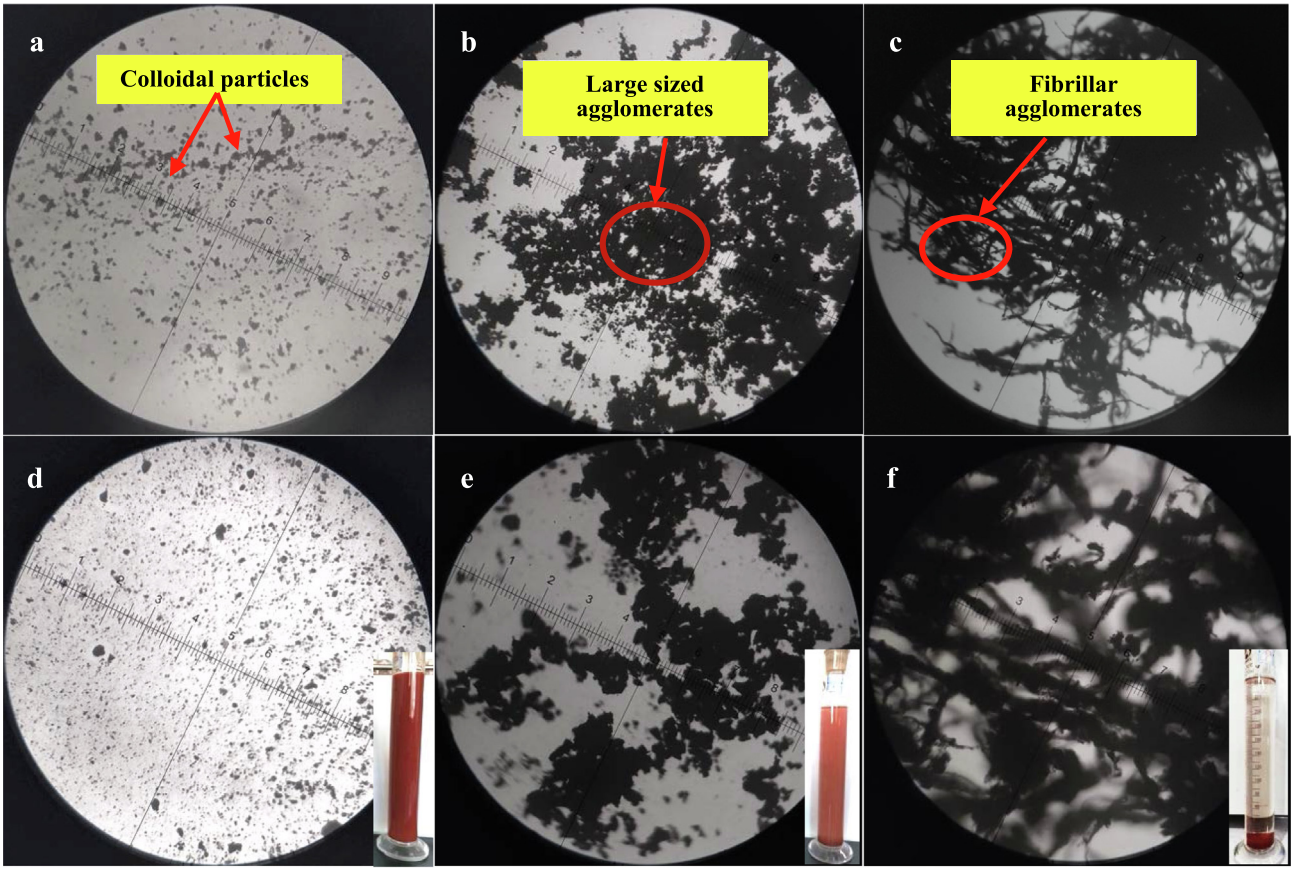

Fig. 7 Micrographs of (a, d) hematite, (b, e) hematite + XG and (c, f) hematite + XG + $FeCl_3 \dot{s} 6H_2O$ at pH 6.4.

and presence of $FeCl_3 \dot{s} 6H_2O$ at pH 6.4, with Fig. 7 showing the morphology of the samples at different magnifications. As can be seen in Fig. 7, it is clearly seen in the microscope image of hematite that showed hematite fine particles are dispersed in deionized water. It is well known that the interactions between fine particles are mainly determined by the electric double layer force. As the zeta potential value on the surface of hematite was negative at pH 6.4 shown in Fig. 4, the electrostatic repulsive forces resulted in the dispersion of fine particles in the solution. However, when hematite was interacted with XG, the microscope images of sample exhibit large sized agglomerates formed, which might be due to the formation of complexes between exposed ferric ions and XG molecule on the surface of hematite. This agrees with the results of FTIR analysis in Fig. 6. More interestingly, as the addition of ferric ions, a larger sized and fibrillar agglomerates were observed as shown in Fig. 7 (c) and (f), which might be due to ferric ions cross-linking with XG at each layer during the formation of Fe-XG where a single ferric ion is bound in between two chains of XG. Similar research about lead ions interacting with XG had also been independently made by others (Bergmann et al., 2008). A single ferric ion is bound between the terminal ends of two XG molecular chains, leading to an intermolecular cross-link and the molecular weight raised rapidly of the overall macromolecule. In this stage, the ferric ions acted as bridges between XG molecules. This means the XG molecular chain is lengthened, and the length of hematite flocs increased. So, the flocs morphology transforms from particles to fibrillar when the XG adsorb on the hematite surface. The larger sized and fibrillar agglomerates are more separable from the solution. This agrees with the results of settling experiments, the addition of XG and $FeCl_3 \dot{s} 6H_2O$ on hematite suspension increases the settling rate. Bridging flocculation is the most common particle aggregation mechanism. It can be clearly observed that the fine hematite particles are adsorbed on the long-chain XG, and this netted structure is also an advantage to the suspending particle deposit by net capture. The main mechanism of XG and Fe^{3+} enhancing settling fine hematite particles is adsorption and bridging.

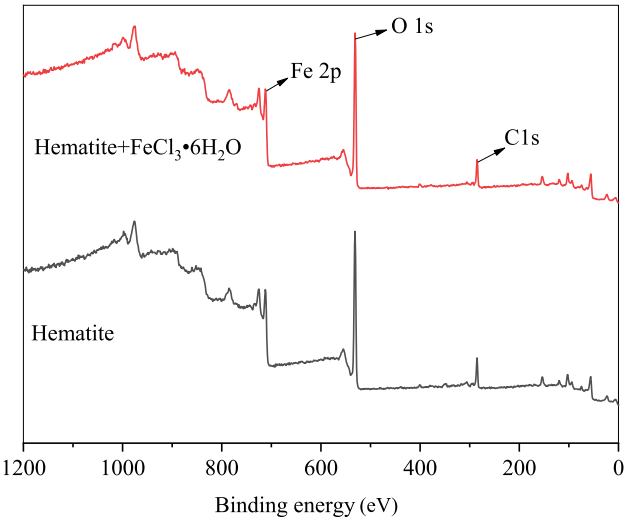

Fig. 8 Hematite and hematite after the reaction of $FeCl_3 \dot{s} 6H_2O$ XPS survey spectra.

3.7. XPS analysis

Coagulants can adsorb on the surface of hematite by chemical complex with exposed ferric ions of hematite during the system of hematite and XG. In contrast, during the system of hematite and XG, $FeCl_3 \dot{s} 6H_2O$ is added to the solution, resulting in differences in the hematite surface environment. The XPS experiment was used to analyze the changes in the chemical environment on the hematite surface before and after the reaction of Fe^{3+}. Fig. 8 shows the XPS survey spectra for hematite and hematite after the reaction of $FeCl_3 \dot{s} 6H_2O$. As shown in Fig. 8, the hematite samples surface contains the expected peaks of O 1 s, Fe 2p and C 1 s which may be caused by carbon dioxide contamination during sample preparation. Table 2 illustrates the changes of the main elements O and Fe on the surface of hematite and hematite after the reaction of $FeCl_3 \dot{s} 6H_2O$. It was found that oxygen is the main element on the hematite surface, with an O/Fe ratio of 45/11, which is relatively close to the other related research (Luo et al., 2016). After hematite was reacted on $FeCl_3 \dot{s} 6H_2O$, the ratio of O/Fe decreased to about 44/11. This suggests that iron ions, as the active sites on the surface of hematite to react with XG, are limited, and the number of active sites of hematite surface increase after the reaction of $FeCl_3 \dot{s} 6H_2O$. That means Fe $(OH)_2^+$, $Fe(OH)^{2+}$ and Fe^{3+} could adsorb on the surface of hematite. This is also the reason that the zeta potential of hematite changed positive with Fe^{3+} added.

Fig. 9 shows Fe 2p XPS spectra of hematite and hematite after the reaction of $FeCl_3 \dot{s} 6H_2O$. The deconvoluted peaks at 711.29 and 724.74 eV are attributed to the Fe oxidation states of Fe $2p_{3/2}$ and $2p_{1/2}$, respectively (Moreira et al., 2017; Dong et al., 2021). The peaks at 718.50 eV and 732.23 eV were attributed to the satellite peaks of Fe $2p_{3/2}$ and $2p_{1/2}$, respectively (Tian et al., 2018). In the spectrum of hematite treated with Fe^{3+}, the binding energy for the spin–orbit splitting peaks of Fe $2p_{3/2}$ and $2p_{1/2}$ are shifted by 0.42 and 0.34 eV, respectively. These large offsets reveal that Fe^{3+} significantly affects the chemical environment of the hematite surface. Significantly, the component of peak 1 increases, and the peak 3 envelope becomes more symmetric, suggesting changes on the surface iron coordination or subtle modifications in the charge state. This shows that Fe-OH was formed on the surface of hematite after the reaction of Fe^{3+} (Moreira et al., 2017; Wei et al., 2019). Additional evidence for this mechanism is provided by the analysis of the O 1 s region.

Table 2 XPS relative atomic concentration of the constituent elements on the surfaces of hematite and hematite after the reaction of $FeCl_3 \dot{s} 6H_2O$.

Samples	Element	Binding energy (eV)	Atomic Concentration (%)
Hematite	C 1 s	285.24	21.09
	O 1 s	531.24	45.54
	Fe 2p	711.57	11.43
Hematite + $FeCl_3 \dot{s} 6H_2O$	C 1 s	285.05	18.00
	O 1 s	530.99	44.40
	Fe 2p	711.44	11.54

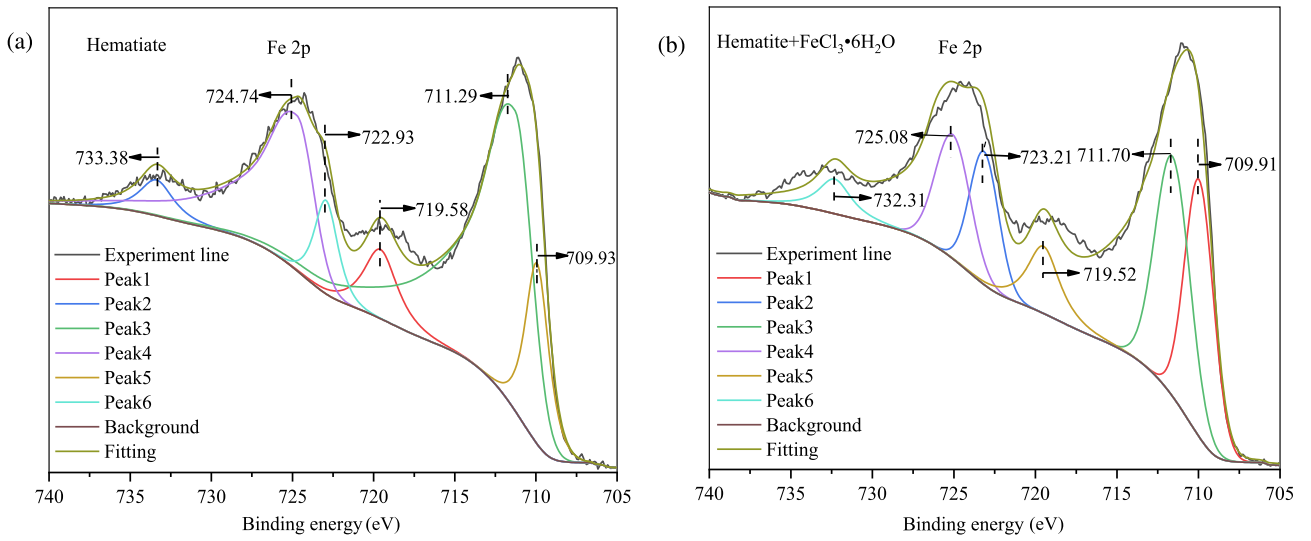

Fig. 9 High-resolution Fe 2p XPS spectra of (a) hematite and (b) hematite after the reaction of $FeCl_3$ś$6H_2O$.

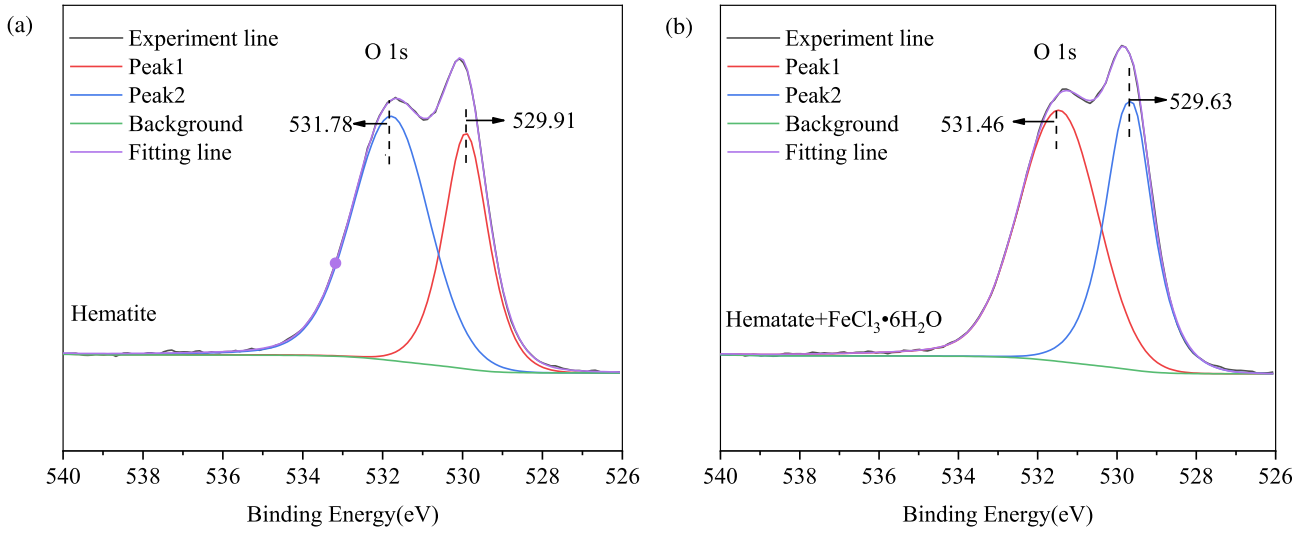

Fig. 10 High-resolution O 1 s XPS spectra of (a) hematite and (b) hematite after the reaction of $FeCl_3$ś$6H_2O$.

The O 1 s core level spectra for hematite and hematite after the reaction of $FeCl_3$ś$6H_2O$ are shown in Fig. 10. The O 1 s of hematite can be deconvoluted into two peaks, these peaks at 529.92 and 531.78 eV are attributed to the oxygen in Fe_2O_3 and the oxygen in water molecules intercalated in the hematite crystal structure or the hydroxyl group (Surf-OH) adsorbed on hematite, respectively (Cheng et al., 2022; Salkar et al., 2019; Salkar et al., 2021). According to the reported, O ls spectra for pure Fe_2O_3 consist of a single peak at approximately 529.9 eV, but a shoulder peak related to adsorbed OH groups may appear depending on the sample preparation conditions (Moreira et al., 2017). This means the hydroxyl group of water bonded to FeO with FeO(OH) formed a hydroxylated hematite surface. The binding energies of O 1 s of hematite decreased from 529.92 to 529.63 eV after the reaction of $FeCl_3$-ś$6H_2O$, which indicated Fe^{3+} adsorbed strongly on the surface of hematite, and the oxygen atoms on the surface of hematite were the adsorption site of $Fe(OH)_2^+$, $Fe(OH)^{2+}$ and Fe^{3+}. In the spectrum of hematite after the reaction of $FeCl_3$ś$6H_2O$, the deconvoluted peaks at 531.78 eV decreased by 0.32 eV, which suggests that $Fe(OH)_2^+$, $Fe(OH)^{2+}$ and Fe^{3+} might be bound to the surface of hematite in the shape of Fe-OH. On the other hand, the persistence of the O1s component indicates that hematite retains its stoichiometry and that hydroxylation is limited.

3.8. Mechanisms of aggregation

The mechanisms, principally bridging, charge neutralization and compressing the thickness of the electric double layer, were proposed in earlier studies (Liu et al., 2021). Based on our experimental results and analysis, we suggest the mechanism of aggregation fine hematite particles suspension using XG in the presence of $FeCl_3$ś$6H_2O$ as shown in Fig. 11. XG

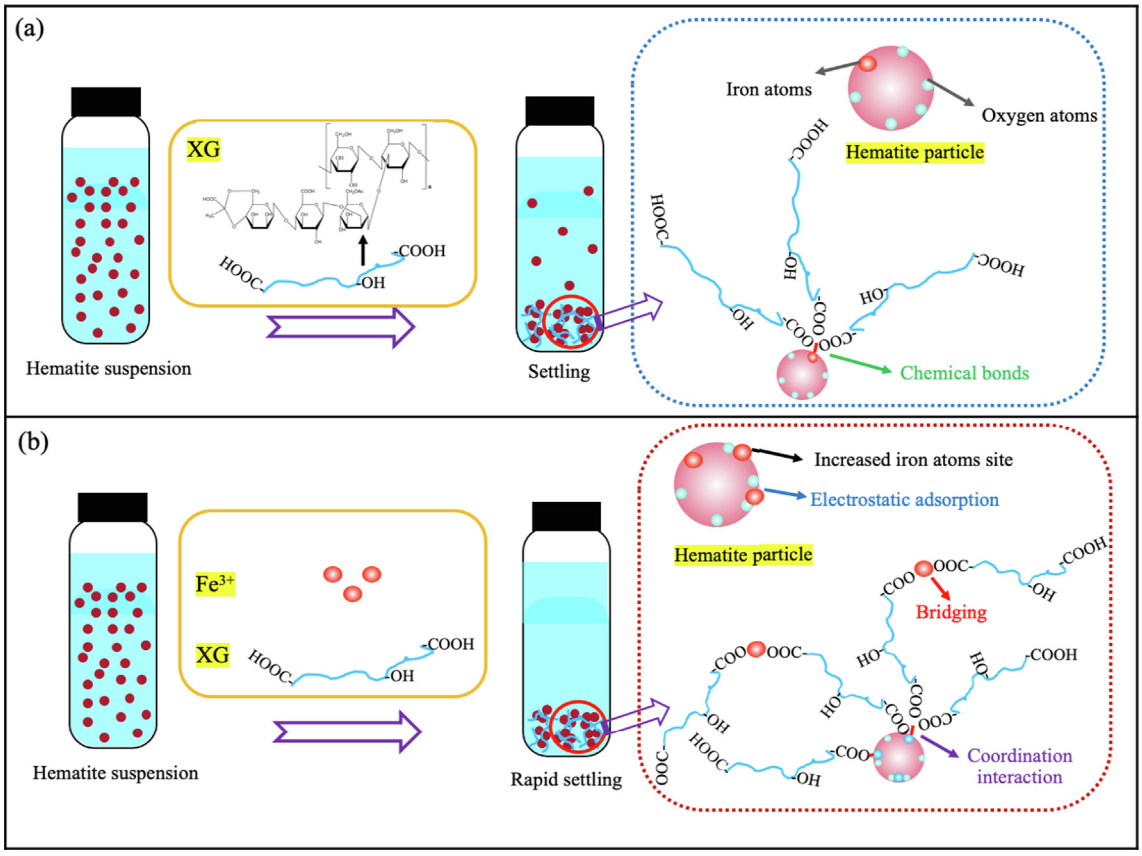

Fig. 11 Graphical illustration of aggregation model of fine hematite particles suspension using XG in the presence of $FeCl_3 \acute{s} 6H_2O$.

and hematite have large negative zeta potential values, suggesting that XG adsorption onto hematite through chemical complexation, and transforming fine hematite particles to settleable agglomerates (Fig. 11 (a)). Loganathan and Sankaran also proposed the same mechanism for the flocculation of iron oxide in the presence of XG (Loganathan and Sankaran, 2021). The adsorption of XG on the hematite surface is attributed to forming the complex between XG molecule and exposed ferric ions on the surface of hematite. However, the amount of XG adsorbed on hematite surface is little, because the active ferric ions sites on the surface of hematite are limited, as supported by the results of the adsorption tests (Fig. 3). Fig. 11 (b) shows that the positively charged $Fe(OH)_2^+$, $Fe(OH)^{2+}$ and Fe^{3+} is bound to the negatively position O^{2-} on the hematite surface by electrostatic adsorption. Moreover, the hematite surface is covered by Fe $(OH)_{3(s)}$ precipitation turned by Fe^{3+}. The adsorption model was usually used to explain the mechanism of the iron ion adsorption on mineral surfaces such as cassiterite and dolomite (Tian et al., 2018; Chen et al., 2022). So, there are more active ferric ions sites on the surface of hematite, leading to more XG molecules adsorption on the hematite surface, as supported by the results of the adsorption tests (Fig. 3). In addition, coordination interaction between ferric ions and XG might also be responsible for the aggregation mechanism. The ferric ions could form a bridge between the hematite particle and XG molecule or XG molecules, and allow the growth of different agglomerates sizes. Consequently, the formation of agglomerates destabilizes the fine hematite particle suspensions and causes rapid settling.

4. Conclusion

In the aggregation settling process of fine hematite particles, the effect of ferric ion and flocculant XG on improving the aggregation of hematite particles was investigated. Based on the results of settling and adsorption experiments and the surface chemical studies, the following conclusions can be drawn. The combined with of XG and Fe^{3+} exhibits high aggregation capacity for the hematite suspension settling than single XG at pH 6.0, and the pH window of high settling has also increased from the pH region of 2–4 to 2–10. The adsorption experiments concerning Fe^{3+} could enhance the adsorption of XG on hematite. The combined with of XG and Fe^{3+} has a stronger co-adsorption on the surface of hematite. Fe^{3+} could adsorb onto hematite surface through forming $Fe(OH)_{3(s)}$ precipitation and electrostatic adsorption of $Fe(OH)_2^+$, $Fe(OH)^{2+}$ and Fe^{3+}, and XG could further adsorb onto hematite surface through specific adsorption with the pre-adsorption of Fe^{3+} active sites. The large sized agglomerates forms in the sample of hematite suspension by adding XG only, while a larger sized and fibrillar agglomerates are observed with the addition of XG and $FeCl_3 \acute{s} 6H_2O$, because the ferric ions could form a bridge among XG molecules based on the coordination interaction between ferric ions active sites and XG, and allow the growth of different agglomerates sizes.

The recovery of fine-grained hematite, where XG play a dominating role in the flocculation of minerals, is significantly affected by the aggregation processing of hematite. To increase fine particle flocculation, boosting the flocculation by Fe^{3+} active sites is the key.

Declaration of Competing Interest

The authors declare the following financial interests/personal relationships which may be considered as potential competing interests: Zhichao Yang reports financial support was provided by the National Natural Science Foundation of China; Qing Teng reports financial support was provided by the Natural Science Foundation of Shanxi Province for Young Scientists, China.

Acknowledgments

The authors acknowledge the financial support of the National Natural Science Foundation of China (51604188) and the Natural Science Foundation of Shanxi Province for Young Scientists, China (No. 20210302124061).

References

Mahmoud H. Abu Elella, Magdy W. Sabaa, Eman Abd ElHafeez, Riham R. Mohamed. Crystal violet dye removal using crosslinked grafted xanthan gum. International Journal of Biological Macromolecules, 137(2019) 1086-1101.

Bergmann, D., Furth, G., Mayer, C., 2008. Binding of bivalent cations by xanthan in aqueous solution. Int. J. Biol. Macromol. 43, 245–251.

Bratskaya, S., Schwarz, S., Liebert, T., Heinze, T., 2005. Starch derivatives of high degree of functionalization 10. flocculation of kaolin dispersions. Colloids Surf. A Physicochem. Eng. Asp. 254, 75–80.

Chen, J., Ao, X., Xie, Y., Yin, Y., 2022. Effects of iron ion dissolution and migration from phosphorite on the surface properties of dolomite. Colloids Surf. A Physicochem. Eng. Asp. 641, 128618.

Cheng, K., Xiqing, W.u., Tang, H., Zeng, Y., 2022. The flotation of fine hematite by selective flocculation using sodium polyacrylate. Miner. Eng. 176, 107273.

Davis, C.C., Edwards, M., 2017. Role of calcium in the coagulation of NOM with ferric chloride. Environ. Sci. Tech. 51, 11652–11659.

Dong, L., Wei, Q., Qin, W., Jiao, F., 2021. Effect of iron ions as assistant depressant of citric acid on the flotation separation of scheelite from calcite. Chem. Eng. Sci. 241, 116720.

Kinga Duczmal, Małgorzata Darowska, Ewa D. Raczyn´ska. Spectral (DFT-IR, FT-IR and UV) similarities and differences between substrate (pyruvate) and inhibitor (oxamate) of lactic dehydrogenase (LDH). Vibrational Spectroscopy, 37 (2005) 77-82.

Ferretti, R., Stoll, S., Zhang, J., Buffle, J., 2003. Flocculation of hematite particles by a comparatively large rigid polysaccharide: schizophyllan. J. Colloid Interface Sci. 266, 328–338.

Jain, V., Tammishetti, V., Joshi, K., Kumar, D., Pradip, B.R., 2017. Guar gum as a selective flocculant for the beneficiation of alumina rich iron ore slimes: density functional theory and experimental studies. Miner. Eng. 109, 144–152.

Kang, M., Oderinde, O., Liu, S., Huang, Q., Ma, W., Yao, F., Guodong, F.u., 2019. Characterization of Xanthan gum-based hydrogel with Fe^{3+} ions coordination and its reversible sol-gel conversion. Carbohydr. Polym. 203, 139–147.

Kumar, D., Jain, V., Rai, B., 2018. Can carboxymethyl cellulose be used as a selective flocculant for beneficiating alumina-rich iron ore slimes? a density functional theory and experimental study. Miner. Eng. 121, 47–54.

Li, M., Xiang, Y., Chen, T., Gao, X., Liu, Q.i., 2021. Separation of ultra-fine hematite and quartz particles using asynchronous flocculation flotation. Miner. Eng. 164, 106817.

Li, D., Yin, W., Sun, C., Yao, J., 2020. Aggregation characteristics of fine hematite and siderite particles in aqueous suspension. Powder Technol. 368, 286–296.

Li, W., Zhou, L., Han, Y., Zhu, Y., Li, Y., 2019. Effect of carboxymethyl starch on fine-grained hematite recovery by high-intensity magnetic separation: experimental investigation and theoretical analysis. Powder Technol. 343, 270–278.

Liang, L., Peng, Y., Tan, J., Xie, G., 2015. A review of the modern characterization techniques for flocs in mineral processing. Miner. Eng. 84, 130–144.

Liu, S., Yao, F., Kang, M., Zhao, S., Huang, Q., Guodong, F.u., 2017. Hierarchical xanthan gum/graphene oxide nanocomposite film induced by ferric ions coordination. Mater. Des. 113, 232–239.

Liu, Y., Zhang, X., Jiang, W., MingRui, W., Li, Z., 2021. Comprehensive review of floc growth and structure using electrocoagulation: Characterization, measurement, and influencing factors. Chem. Eng. J. 417, 129310.

Loganathan, S., Sankaran, S., 2016. Surface chemical properties and selective flocculation studies on alumina and silica suspensions in the presence of xanthan gum. Miner. Eng. 98, 213–222.

Loganathan, S., Sankaran, S., 2021. Surface chemical and selective flocculation studies on iron oxide and silica suspensions in the presence of xanthan gum. Miner. Eng. 160, 106668.

Luo, X.-M., Yin, W.-Z., Wang, Y.-F., Sun, C.-Y., Ma, Y.-Q., Liu, J., 2016. Effect and mechanism of dolomite with different size fractions on hematite flotation using sodium oleate as collector. J. Central South Univ. 23, 529–534.

McGuire, M.J., Addai-Mensah, J., Bremmell, K.E., 2006. The effect of polymer structure type, pH and shear on the interfacial chemistry, rheology and dewaterability of model iron oxide dispersions. Colloids Surf. A Physicochem. Eng. Asp. 275, 153–160.

Mittal, H., Alili, A.A., Morajkar, P.P., Alhassan, S.M., 2021. Graphene oxide crosslinked hydrogel nanocomposites of xanthan gum for the adsorption of crystal violet dye. J. Mol. Liq. 323, 115034.

Moreira, G.F., Peçanha, E.R., Monte, M.B.M., Leal, L.S., Filho, F.S., 2017. XPS study on the mechanism of starch-hematite surface chemical complexation. Miner. Eng. 110, 96–103.

Lopamudra Panda, PradipK. Banerjee, Surendra Kumar Biswal, R. Venugopal, N.R. Mandre. Performance evaluation for selectivity of the flocculant on hematite in selective flocculation. International Journal of Minerals, Metallurgy and Materials, 20 (2013) 1123-1129.

Poorni, S., Natarajan, K.A., 2014. Flocculation behaviour of hematite–kaolinite suspensions in presence of extracellular bacterial proteins and polysaccharides. Colloids Surf. B Biointerfaces 114, 186–192.

Meysam Rahbari, Mehran Kianirad, Seyed Mohammad Heydarian, Seyed Saeed Mirdamadi. Effects of pH and Fe(III) Concentrations in Xanthan Gum Treatments on Soil Penetrability Resistance. Soil Science Society of America Journal 81(2017) 775-780.

Salam, W., El Aref, M., Gaupp, R., 2015. Spectroscopic characterization of iron ores formed in different geological environments using FTIR, XPS, Mössbauer spectroscopy and thermoanalyses. Spectrochim. Acta A Mol. Biomol. Spectrosc. 136, 1816–1826.

Salkar, A.V., Fernandes, R.X., Bhosale, S.V., Morajkar, P.P., 2019. NH- and CH-substituted ureas as self-assembly directing motifs for facile synthesis and electrocapacitive applications of advanced WO_{3-x} one-dimensional nanorods. ACS Appl. Energy Mater. 2, 8724–8736.

Salkar, A.V., Naik, A.P., Bhosale, S.V., Morajkar, P.P., 2021. Designing a rare DNA-like double helical microfiber superstructure via self-assembly of in situ carbon fiber-encapsulated WO_{3-x} nanorods as an advanced supercapacitor material. ACS Appl. Mater. Interfaces 13, 1288–1300.

Sato, D., Kobayashi, M., Adachi, Y., 2004. Effect of floc structure on the rate of shear coagulation. J. Colloid Interface Sci. 272, 345–351.

Tang, X., Huang, T., Zhang, S., Wang, W., Zheng, H., 2020. The role of sulfonated chitosan-based flocculant in the treatment of hematite T wastewater containing heavy metals. Colloids Surf. A Physicochem. Eng. Asp. 585, 124070.

Tian, M., Liu, R., Gao, Z., Chen, P., Han, H., Wang, L.i., Zhang, C., Sun, W., Yuehua, H.u., 2018. Activation mechanism of Fe (III) ions in cassiterite flotation with benzohydroxamic acid collector. Miner. Eng. 119, 31–37.

Wang, L., Zhou, W., Song, S., Gao, H., Niu, F., Zhang, J., Ai, G., 2021. Selective separation of hematite from quartz with sodium oleate collector and calcium lignosulphonate depressant. J. Mol. Liq. 322, 114502.

Wei, Q., Dong, L., Jiao, F., Qin, W., 2019. Use of citric acid and Fe (III) mixture as depressant in calcite flotation. Colloids Surf. A Physicochem. Eng. Asp. 578, 123579.

Weissenborn, P.K., 1996. Behaviour of amylopectin and amylose components of starch in the selective flocculation of ultrafine iron ore. Int. J. Miner. Process. 47, 197–211.

Yang, Z., Wang, W., Liu, S., 2017. Flocculation of coal waste slurry using bioflocculant produced by Azotobacter chroococcum. Energy Fuels 31, 1460–1467.

Yang, Z., Teng, Q., Han, Y., Zhang, G., Fang, S.U., 2023. New insights into the combination of Fe(III) and Xanthan gum in dewatering of coal slurry: molecular self-assembly. Fuel 332, 126205.

Yue, T., Xiqing, W.u., Chen, X., Liu, T., 2018. A study on the flocculation and sedimentation of iron tailings slurry based on the regulating behavior of Fe^{3+}. Minerals 8, 421.

Zhang, W., Jian, W., Weng, L., Zhang, H., Zhang, J., Anbo, W., 2020. An improved phenol-sulfuric acid method for the determination of carbohydrates in the presence of persulfate. Carbohydr. Polym. 227, 115332.

Zhang, X., Yangge Zhu, Y.u., Xie, Y.S., Zheng, G., 2017. A novel macromolecular depressant for reverse flotation: synthesis and depressing mechanism in the separation of hematite and quartz. Sep. Purif. Technol. 186, 175–181.